Cryogenics. 50(11-12), 765-771 (2010)

Simulation for prediction of distribution of critical current among specimens under low applied bending strains near the average irreversible strain in Bi2223 composite tape

S. Ochiai[1a,*] M. Fujimoto[1], H. Okuda[1], S. S. Oh[2] and D. W. Ha[2]

[1] *Department of Materials Science and Engineering, Graduate School of Engineering, Kyoto University, Sakyo-ku, Kyoto 606-8501, Japan*

[2] *Korea Electrotechnology Research Institute, 28-1 Sungju-Dong, Changwon 641-120, Korea*

Abstract

When many multi-filamentary Bi2223 composite specimens with different irreversible bending strain to each other are tested, number of damaged specimens among all increases with bending strain in the low bending strain region near the average irreversible strain. The present work attempted to predict the distribution of critical current among many specimens in such a low bending strain region with a proposed simulation method that uses the damage evolution model, Monte Carlo method and the experimental data measured at limited strains. With the proposed simulation method, statistical features in variation of distribution of critical current values among specimens near the average irreversible bending strain were elucidated.

Keywords: Superconductors (A); critical current density (C), Stress effects (C)

* Corresponding author, fax: +81 75 753 4841
E-mail address: shojiro.ochiai@materials.mbox.media.kyoto-u.ac.jp (S. Ochiai)

1. Introduction

Under tensile/bending applied strain, critical current of Bi2223 composite tape is reversible up to the irreversible strain at which the damage of the Bi2223 filaments takes place first, but beyond the irreversible strain, the critical current decreases irreversibly with increasing applied strain due to the damage evolution[1-13]. The irreversible strain and the relation of critical current to applied strain are different among specimens due to the difference in damage evolution [1-9]. For reliability and safe design, it is needed to develop a description method of the critical current distribution among specimens near the average irreversible strain.

In bent samples, filaments are damaged when the tensile strain along a sample length direction reaches the tensile fracture strain of the filaments embedded in the composite tape, given by ε_f-ε_r where ε_f and ε_r are the tensile fracture- and residual- strains of the filaments, respectively [7-10, 15]. Recently, the authors have proposed a damage evolution model for analysis of distribution of critical current [7-9], in which the difference in the damage evolution among the specimens was expressed by the distributed ε_f-ε_r values in combination with the shape of the core (the region in which Bi2223 filaments are bundled into Ag). With this model, the measured distribution of the normalized critical current (I_c/I_{c0} where I_c and I_{c0} are the critical current values at arbitrary and zero bending strains, respectively) was described well. However, the distribution of I_c-values could not be described in that form.

The aim of the present work is to develop a simulation method for prediction of the distributions both of I_c and I_c/I_{c0} values among many specimens in bent Bi2223 multifilamentary composite tape by extending the approach in our preceding work [7-9] and to elucidate the change in distributions of I_c and I_c/I_{c0} values in low bending strain region where the number of damaged specimens increases with increasing strain due to the distributed irreversible strain.

2. Experimental procedure

The multifilamentary Bi2223/Ag/Ag alloy composite tape, fabricated by the powder-in-tube method at Korea Electrotechnology Research Institute (KERI), was used as the experimental sample. It contained 55 Bi2223 filaments. The thickness t and width W of

the sample were 0.23 and 4.1 mm, respectively.

Figure 1(a) shows the as-observed transverse cross-section of the sample [8]. When the thickness direction is enlarged by a factor of 3, the shape of the core can be more clearly observed, as shown with a broken curve in Fig.1(b). As the damage of the Bi2223 filaments existing in the core causes the reduction in critical current, it is necessary to formulate the shape. Taking the width- and thickness- directions of the composite tape as the x- and y- axes, respectively, and the center of the composite tape as $x=y=0$ (Fig.1(c)), and denoting the y-coordinate of the boundary of the core (ABCDEFGHA in Fig.1(c)) as y_{core}, we formulated y_{core} as a function of x by 9th order polynomials, as follows [8,15]. The length unit is mm.

$$\left.\begin{aligned} &\text{CDE in Fig.1: } y_{core} = 0.0660214 - 0.0405173x + 1.03050x^2 - 4.05239x^3 \\ &\qquad + 8.94014x^4 - 12.6431x^5 + 11.3895x^6 - 6.22952x^7 \\ &\qquad + 1.87094x^8 - 0.235769x^9 \qquad \text{for } 0 \le x \le 1.95 \\ &\text{ABC: symmetry with EDC with respect to } x=0 \\ &\text{AHGFE: symmetry with ABCDE with respect to } y=0 \end{aligned}\right\} \quad (1)$$

Equation (1) is used later in Subsection 3.2 for description of the damage evolution and its relation to critical current.

For measurement of critical current I_c under bending strain, the bending strain ε_B ($=t/(2R)$, where t is the sample thickness (0.23 mm) and R is the radius of dies used to bend specimens, was given to the test specimens by 0 % with straight dies ($R=\infty$) and 0.338 % with dies of R=34.0 mm at room temperature. The I_c (and I_c/I_{c0}) values at $\varepsilon_B=0$ and 0.338 % were measured for 36 test specimens at 77K in a self-field with a 1 μV/cm criterion. In addition, the I_c values at ε_B=0.290 % were measured using dies with R=19.8 mm for 48 test specimens. The results at ε_B=0.290 % are used to examine the simulation result in Subsection 3.3.

3. Results and discussion

3.1 Description of measured I_c- and I_c/I_{c0}- values by regression analysis using three-parameter Weibull distribution function

Figure 2(a, b, c) show the probability density f of the measured I_c values at ε_B=0, 0.290 and 0.338 %, respectively. The average critical current values, $I_{c,ave}$, were 69.1, 66.0 and 62.7 A, respectively. Figure 3 shows the change of $I_{c,ave}$ with ε_B. The open circles show the present result and the triangles show the values taken from our former work [15]. The solid curve shows the $I_{c,ave}$–ε_B relation analyzed by the damage evolution model [7-9], whose details are shown later in Subsection 3.2. The average irreversible bending strain $\varepsilon_{B,irr,ave}$ was 0.243%. The experimental results were described well by the damage evolution model. The variation of distribution of I_c values with ε_B in the low strain region (ε_B =0-0.37% covering $\varepsilon_{B,irr,ave}$=0.243 % in a rectangle in Fig.3) is analyzed in detail in Subsection 3.3.

Distribution of I_c values was formulated with the three-parameter Weibull distribution function [16], according to which the cumulative probability F of I_c is expressed by

$$F(I_c) = 1 - \exp\left\{-\left(\frac{I_c - I_{c,min}}{I_0}\right)^m\right\} \qquad (2)$$

where $I_{c,min}$ is the minimum (lower limit) critical current, I_0 is the scale parameter and m is the shape parameter. From the regression analysis of experimental results with Eq.(2), it was found that $I_{c,min}$=63.2, 55.2 and 53.4 A give the highest linearity between $\ln\ln(1-F)^{-1}$ and $\ln(I_c-I_{c,min})$ for the experimental results at ε_B=0, 0.290 and 0.338%, respectively, as shown in Fig.2(a', b' ,c'). The estimated parameters of ($I_{c,min}$, m, I_0) for the distribution of measured I_c-values at ε_B=0, 0.290 and 0.338% were (63.2A, 5.85, 6.37A), (55.2A, 5.32, 11.7A) and (53.4A, 3.87, 10.3A), respectively. With these estimated parameter values, the cumulative probability F expressed by Eq. (2) was converted to the density probability f (frequency). The calculated f- I_c relations are presented with solid curves in Fig.2(a,b,c), describing well the experimental results.

Probability density f of I_c/I_{c0} values measured at ε_B=0.338 % is shown in Fig.4(a). The cumulative probability $F(I_c/I_{c0})$ with the three-parameter Weibull distribution is expressed as

$$F(I_c/I_{c0}) = 1 - \exp\left\{-\left(\frac{I_c/I_{c0} - (I_c/I_{c0})_{\min}}{(I_c/I_{c0})_0}\right)^m\right\} \qquad (3)$$

where $(I_c/I_{c0})_{min}$, m and $(I_c/I_{c0})_0$ are the lower limit of I_c/I_{c0} value, shape parameter and scale parameter, respectively. In a similar manner to the analysis of distribution of I_c, the parameter values in Eq.(3) that fit to the experimental result were estimated by the regression analysis. We had $(I_c/I_{c0})_{min}$=0.715, m=6.06 and $(I_c/I_{c0})_0$=0.207. The three-parameter Weibull distribution was suitable also for description of I_c/I_{c0} values, as shown by the high linearity between $\ln\ln(1-F)^{-1}$ and $\ln(I_c/I_{c0}-0.715)$ (Fig.4(b)).

The estimated distribution functions are used in Subsection 3.3 to examine whether the present simulation can reproduce well the experimental results or not.

3.2 Estimation of distribution functions of the ε_f-ε_r and $\varepsilon_{B,irr}$ values

The relation of geometry of the cross-section to damage evolution is schematically shown in Fig.1(c). When ε_B reaches $\varepsilon_{B,irr}$, damage to reduce critical current takes place in the outermost filaments existing at the maximum value of y_{core} (Eq.(1)), $y_{core,max}$ (=0.101 mm in the present sample). When ε_B is raised from $\varepsilon_{B,irr}$ to $\varepsilon_{B,i}$ and then to $\varepsilon_{B,i+1}$, the damage front y_f moves from $y_{core,max}$ to $y_{f,i}$ and then to $y_{f,i+1}$, resulting in reduction of the cross-sectional area of the Bi2223 filaments and hence of critical current. According the damage evolution model [7-9], $\varepsilon_{B,irr}$ and I_c/I_{c0} are expressed by using the ε_f-ε_r value and Eq.(1), as follows.

$$\varepsilon_{B,irr} = \left(\frac{t/2}{y_{core,max}}\right)(\varepsilon_f - \varepsilon_r) \qquad (4)$$

$$\left.\begin{aligned} \frac{I_c}{I_{c0}} &= 1 \quad \text{for } \varepsilon_B \le \varepsilon_{B,irr} \\ \frac{I_c}{I_{c0}} &= 1 - 2\int_0^{W_{core}/2}\left\{y_{core} - \frac{(\varepsilon_f - \varepsilon_r)(t/2)}{\varepsilon_B}\right\}\frac{dx}{A_{core}} \quad \text{for } \varepsilon_B \ge \varepsilon_{B,irr} \end{aligned}\right\} \qquad (5)$$

where A_{core} is the cross-sectional area of the core and W_{core} is the width of the core (distance between A and E in Fig.1(c)). As the ε_f-ε_r values are distributed among specimens, the $\varepsilon_{B,irr}$- and I_c/I_{c0}- values are also distributed among specimens (Eqs.(4) and (5)).

If the distribution function of ε_f-ε_r is known in advance, the distributions of $\varepsilon_{B,irr}$ and I_c/I_{c0} can be calculated by Eqs.(4) and (5), respectively, with y_{core} given by Eq.(1) and the measured geometrical values of $y_{core,max}$=0.101 mm, t=0.230 mm, A_{core}=0.660 mm^2 and W_{core}=3.90mm. However, the distribution of ε_f-ε_r values is unknown. In the present work, the ε_f-ε_r values were back-calculated by substituting the measured I_c/I_{c0} values at ε_B=0.338 % and the geometrical factors mentioned above into Eq.(5). The probability density $f(\varepsilon_f$-$\varepsilon_r)$ of the obtained ε_f-ε_r values are presented in Fig.5(a).The average of ε_f-ε_r values, $(\varepsilon_f$-$\varepsilon_r)_{ave}$, was 0.214%. The estimated ε_f-ε_r values were formulated also by the three-parameter Weibull distribution function, expressed by

$$F(\varepsilon_f-\varepsilon_r)=1-\exp\left\{-\left(\frac{\varepsilon_f-\varepsilon_r-(\varepsilon_f-\varepsilon_r)_{min}}{(\varepsilon_f-\varepsilon_r)_0}\right)^m\right\} \qquad (6)$$

where $F(\varepsilon_f$-$\varepsilon_r)$ is the cumulative probability, and $(\varepsilon_f$-$\varepsilon_r)_{min}$, ε_0 and m are the minimum value of ε_f-ε_r, scale parameter and shape parameter, respectively. The parameters ($(\varepsilon_f$-$\varepsilon_r)_{min}$, ε_0 and m) for the distribution of ε_f-ε_r values were estimated by the regression analysis to be 0.130%, 0.0928 % and 4.19, respectively. The estimated parameter values describe the experimental results as shown with a solid curve in Fig.5(a) and give a high linearity between $\ln\ln(1-F)^{-1}$ and $\ln\{\varepsilon_f$-ε_r-$(\varepsilon_f$-$\varepsilon_r)_{min}\}$ as shown in Fig.5(b).

The relation of ε_f-ε_r to $\varepsilon_{B,irr}$ is expressed by Eq.(4). Substituting ε_f-ε_r=$\varepsilon_{B,irr}y_{core,max}/(t/2)$ derived from Eq.(4) into Eq.(6), we have the cumulative distribution function of $\varepsilon_{B,irr}$;

$$F(\varepsilon_{B,irr})=1-\left\langle-\left[\left\{\frac{y_{core,max}/(t/2)}{(\varepsilon_f-\varepsilon_r)_0}\right\}\left\{\varepsilon_{B,irr}-\frac{(\varepsilon_f-\varepsilon_r)_{min}}{y_{core,max}/(t/2)}\right\}\right]^m\right\rangle \qquad (7)$$

Substituting $y_{core,max}$=0.101 mm, $(\varepsilon_f-\varepsilon_r)_{min}$=0.130%, m =4.19, ε_0=0.0928 % and t=0.230 mm into Eq.(7), we have the cumulative distribution $F(\varepsilon_{B,irr})$ of $\varepsilon_{B,irr}$ for the present sample as shown in Fig.6. The average of $\varepsilon_{B,irr}$ values, $\varepsilon_{B,irr,ave}$, was 0.243%. When many specimens whose ε_f-ε_r values obey Eq.(6) are tested, the specimen with the lowest ε_f-ε_r value ($(\varepsilon_f-\varepsilon_r)_{min}$=0.130 %) at $y_{core,max}$ is damaged first among all specimens when ε_B reaches its $\varepsilon_{B,irr}$-value ($=\varepsilon_{B,irr,min}=(\varepsilon_f-\varepsilon_r)_{min}(t/2)/y_{core,max}$)=0.148 %). No specimen is damaged up to ε_B=0.148 %. The number of damaged specimens increases with increasing ε_B, in accordance with increase in $F(\varepsilon_{B,irr})$. At ε_B, the specimens whose $\varepsilon_{B,irr}$ values are lower than ε_B have been damaged. The fraction of the damaged specimens F_d(=ratio of the damaged specimens to all specimens) at ε_B is calculated by replacing $\varepsilon_{B,irr}$ by ε_B in Eq.(7). Namely, the $F_d(\varepsilon_B)$- ε_B curve is the same as $F(\varepsilon_{B,irr})$- $\varepsilon_{B,irr}$ one. Accordingly, as indicated in Fig.6, at ε_B=0.20, 0.24, 0.29 and 0.32 % for instance, the fractions F_d of the damaged specimens increase to 0.051, 0.435, 0.97 and 0.9996, respectively. $F_d(\varepsilon_B)$- ε_B curve in Fig.6 shows that, in the range of low bending strain (0-0.37% in this work, in which $\varepsilon_{B,irr,ave}$=0.243% is included), there exist three regions where no specimen is damaged (region (i) for ε_B=0–0.15%), damaged and non-damaged specimens co-exist (region (ii) for ε_B=0.15–0.32%) and almost all specimens are damaged (ε_B=0.32–0.37%).

3.3 Monte Carlo simulation to predict the distribution of I_c/I_{c0} and I_c values at arbitrary bending strain from the distribution of original critical current I_{c0} and distribution of ε_f-ε_r values estimated from the distribution of I_c/I_{c0} values measured at ε_B=0.338 %

The distributions of the I_c/I_{c0} and I_c values were simulated by the following procedure in which the distributed ε_f-ε_r values given by Eq.(6) were combined with Eq.(5). As a first approximation, the distribution function of ε_f-ε_r at ε_B=0.338 % was used for simulation of distribution of I_c–values at arbitrary bending strain in low bending strain range (ε_B=0-0.37%).

(1) Determination of ε_f-ε_r value of the i-specimen, $(\varepsilon_f\text{-}\varepsilon_r)_i$, where i is the specimen number among the total number 300 of simulated specimens: A random value $R(i)$ was generated in the computer. Setting $F(\varepsilon_f\text{-}\varepsilon_r)=R(i)$ and substituting the estimated values of $(\varepsilon_f\text{-}\varepsilon_r)_{min}$=0.130 %, m=4.19 and ε_0=0.0928 % in Eq.(6), we had the ε_f-ε_r value of the i-specimen, $(\varepsilon_f\text{-}\varepsilon_r)_i$.

(2) Determination of I_c/I_{c0} value of the i-specimen, $(I_c/I_{c0})_i$: As shown in Subsection 3.2, at a given ε_B, the specimens with ε_f-ε_r values lower than $\varepsilon_B y_{core,max}/(t/2)$ have been damaged but not those with ε_f-ε_r values higher than it. In accordance with such a situation, when the $(\varepsilon_f\text{-}\varepsilon_r)_i$ value obtained in (1) was higher than $\varepsilon_B y_{core,max}/(t/2)$, the $(I_c/I_{c0})_i$ was set to be 1 (unity). When the $(\varepsilon_f\text{-}\varepsilon_r)_i$ was lower than $\varepsilon_B y_{core,max}/(t/2)$, the $(\varepsilon_f\text{-}\varepsilon_r)_i$ value, y_{core}(Eq.(1)), ε_B value and t=0.23 mm were substituted into Eq.(5) and the I_c/I_{c0} value of the i-specimen was calculated.

(3) Determination of the I_c value of the i-specimen, $(I_c)_i$: Figure 7 shows the plot of measured I_c-value at ε_B=0.338 % against the original critical current I_{c0} (=I_c at ε_B=0%) for each specimen. The I_c values are almost independent of I_{c0} values. This suggests that the damage at ε_B=0.338 % took place almost evenly for high- and low- I_{c0} specimens and the correlation between the damage behavior and I_{c0} value is, if exists, small. The same feature has been observed for the sample from different supplier [7]. Based on these experimental results, the $I_{c0,i}$ value was treated to be independent of $I_{c,i}$ in the present simulation. The $I_{c0,i}$ value of the i-specimen was obtained by generating another random value $R'(i)$ different from $R(i)$, setting $F(I_{c0}(=I_c$ at ε_B=0%))=$R'(i)$ and substituting the estimated values of $I_{c,min}$=63.2A, m=5.85 and I_0=6.37A for distribution of I_{c0} into Eq.(2). Then, the $I_{c,i}$ value was obtained from the values of $(I_c/I_{c0})_i$ and $I_{c0,i}$.

(4) Determination of $(I_c/I_{c0})_i$ and $I_{c,i}$ values for i=1 to 300 at eB=0 to 0.37%: The procedure (1) to (3) were repeated for 300 times, and $(I_c/I_{c0})_i$ and $I_{c,i}$ values (i=1 to 300) were obtained for a given ε_B. Such a simulation was carried out for ε_B=0, 0.15, 0.17, 0.20, 0.23, 0.26, 0.29, 0.32, 0.338, 0.35 and 0.37%.

Figure 8 shows the representative simulation results for probability density f of the I_c and I_c/I_{c0} values, respectively. The regression curves of the experimental results (solid curves

in Fig.2(a), (b), and (c) for I_c values at ε_B=0, 0.290 and 0.338 % and a solid curve in Fig.4(a) for I_c/I_{c0} values at ε_B=0.338 %) are redrawn with solid curves in Fig.8, for comparison. The experimental results were reproduced well. It is noted that the measured distribution of I_c values at ε_B=0.29 % was described well, despite that the distribution of ε_f-ε_r values estimated from the experimental data of I_c/I_{c0} values at ε_B=0.338 % was used for simulation. This suggests that the distribution of ε_f-ε_r values estimated at a limited bending strain can be employed without serious loss of accuracy for simulation to predict the distribution of I_c (and I_c/I_{c0}) values at other bending strains, when the bending strain range in simulation is near to the bending strain at which ε_f-ε_r values are estimated.

The variations of simulated average of I_c, $I_{c,ave}$, and average of I_c/I_{c0}, $(I_c/I_{c0})_{ave}$, with ε_B are shown in Fig.9(a). The open circles show the measured $I_{c,ave}$ values for comparison. The solid curve shows the $I_{c,ave}$–ε_B relation calculated by substituting y_{core} (Eq.(1)), $I_{c0,ave}$=69.1 A, $\varepsilon_{B,irr,ave}$=0.243 %, $(\varepsilon_f$-$\varepsilon_r)_{ave}$=0.214 %, $y_{core,max}$=0.101 mm, t=0.230 mm, A_{core}=0.660 mm^2, W_{core}=3.90mm into Eq.(5). This curve corresponds to the assumed case where all specimens have a common unique value of ε_f-ε_r=0.214% that corresponds to $\varepsilon_{B,irr}$=0.243 % (Eq.(4)).

In experiment, the coefficient of variation (COV=average/standard deviation) of critical current, COV(I_c), was measured to be 0.0165, 0.0383 and 0.0427 at ε_B=0, 0.290 and 0.338 %, respectively. The COV of normalized critical current, COV(I_c/I_{c0}), is zero at ε_B=0 %. It increased to 0.0400 at ε_B=0.338%. Both COV(I_c) and COV(I_c/I_{c0}) increased largely due to the difference in damage evolution among test specimens. The variation of COV(I_c) with increasing ε_B is also an important item for reliability and safe design. The measured and simulated COV(I_c) and COV(I_c/I_{c0}) values are plotted against ε_B in Fig.9(b). The following statistical features in the low bending strain range are read from Figs.9(a) and (b).

(A) The $I_{c,ave}$-ε_B and $(I_c/I_{c0})_{ave}$-ε_B curves for ε_B=0.15 to around 0.30 % (broken curve in Fig.9(a)) simulated statistically with distributed ε_f-ε_r values with an average of $(\varepsilon_f$-$\varepsilon_r)_{ave}$=0.214%, are lower than the curves calculated non-statistically with a fixed value of

$(\varepsilon_f\text{-}\varepsilon_r)_{ave}$=0.214% (solid curve). In the statistically analyzed $I_{c,ave}$-ε_B and $(I_c/I_{c0})_{ave}$-ε_B curves, the $I_{c,ave}$ and $(I_c/I_{c0})_{ave}$ values flatten off and approach 1(unity) asymptotically with decreasing ε_B. The minimum irreversible strain $\varepsilon_{B,irr,min}$ for distributed ε_f-ε_r is calculated to be 0.148% for $(\varepsilon_f\text{-}\varepsilon_r)_{min}$=0.130 % (Eq.(4)), which is by 0.09% lower than $\varepsilon_{B,irr,ave}$. The largest difference in $I_{c,ave}$ (and $(I_c/I_{c0})_{ave}$) between the statistical simulation and non-statistical calculation is found at around $\varepsilon_B=\varepsilon_{B,irr,ave}$=0.243% at which around half of specimens are damaged (Fig.6). When ε_B exceeds 0.3% where most specimens are damaged, the difference in $I_{c,ave}$ (and $(I_c/I_{c0})_{ave}$) between them becomes small.

(B) COV(I_c) and COV(I_c/I_{c0}) can be obtained by the statistical simulation but not by the non-statistical calculation. The present statistical simulation revealed the following features for the variation of COV(I_c) and COV(I_c/I_{c0}) with ε_B. (a) Both COV(I_c) and COV(I_c/I_{c0}) start to increase at $\varepsilon_B=\varepsilon_{B,irr,min}$. (b) The COV($I_c$) and COV($I_c/I_{c0}$) increase significantly with ε_B in the neighborhood of $\varepsilon_{B,irr,ave}$ in accordance with the increase in fraction F_d of damaged specimens. (c) The COV(I_c) is affected by the distribution of I_{c0} and that of extent of damage, while COV(I_c/I_{c0}) is affected by the latter distribution. Accordingly, the COV(I_c) is higher than COV(I_c/I_{c0}) in the whole range of bending strain. (d) The difference between COV(I_c) and COV(I_c/I_{c0}) becomes small at high applied strain (>0.3%), suggesting that the COV for both I_c and I_c/I_{c0} values at high bending strains is governed mainly by the difference in damage evolution among specimens.

4. Conclusions

(1) A simulation method was proposed for prediction of the distribution of I_c-values among many specimens at arbitrary bending strain within 0 ~ 0.37%, based on the damage evolution model that uses measured distribution of the normalized critical current (I_c/I_{c0}) -values at a bending strain (0.338%) and the distribution of the measured original critical current (I_{c0}) values at zero bending strain. With this method, the experimental results for the measured I_c-values were reproduced well in the computer.

(2) The simulation method proposed in (1) was applied for description of the I_c- and I_c/I_{c0}-

values near the average irreversible bending strain. The decreasing behavior of the average I_c- and I_c/I_{c0} values and the increasing behavior of the coefficient of variation of I_c- and I_c/I_{c0} values in the transition bending strain range where the fraction of damaged specimens increases were described satisfactorily.

ACKNOWLEDGEMENTS

The authors wish to express their gratitude to The Ministry of Education, Culture, Sports, Science and Technology, Japan, for a grant-in-aid for scientific research (no.22360281).

References

[1] van Eck H J N, Vargast V, ten Haken B, ten Kate H H. Bending and axial strain dependence of the critical current in superconducting BSCCO tapes. Supercond. Sci. Technol. 2002;15(8):1213-5.

[2] Kitaguchi K, Itoh K, Kumakura H, Takeuchi T, Togano K, Wada H. Strain effect in Bi-based oxide/Ag superconducting tapes. IEEE Trans. Appl. Supercond. 2001;11(1): 3058-61.

[3] Wang Y, Lu Y, Xu X, Dai S, Hui D, Xiao L, Lin L. Detecting and describing the inhomogeneity of critical current in practical long HTS tapes using contact-free method. Cryogenics 2007;47(4):225-31.

[4] Katagiri K, Shin H S, Kasaba K, Tsukinokizawa T, Hiroi K, Kuroda K, Itoh K, Wada H. Local variations in the critical current degradation of Ag/Bi2223 tape by tensile and bending strains. Supercond. Sci. Technol. 2003;16(9):995-9.

[5] Kuroda T, Itoh K, Katagiri K, Goldacker W, Hasessler W, ten Haken B, Kiuchi M, Noto N, Ochiai S, Otabe S, Shin H S, Sosnowski J, Weijers H, Wada H, Kumakura K. Bending strain effect on critical current of Bi-2223 superconductor tapes—report of international round-robin-test. Physica C 2005; 425(3-4):111-20.

[6] Shin H S, Katagiri K. Critical current degradation behavior in Bi-2223 superconducting tapes under bending and torsion strains. Supercond. Sci. Tecnol. 2003;16(9):1012-8.

[7] Ochiai S, Shin J K, Okuda H, Sugano M, Hojo M, Osamura K, Kuroda T, Itoh K, Wada H. Analysis of the distribution of critical current of bent Bi2223 composite tape based on

a unifying parameter approach. Supercond. Sci. Technol. 2008;21(5):054002.

[8] Ochiai S, Fujimoto M, Shin J K, Okuda H, Oh S S, Ha D W. Distribution of normalized critical current of bent multifilamentary Bi2223 composite tape J. Appl. Phys. 2009;106(10):103916.

[9] Ochiai S, Okuda H, Sugano M, Hojo M, Osamura K, Kuroda T, Itoh K, Kitaguchi H, Kumakura H, Wada H. Analysis of critical current distribution of bent Bi2223 composite tapes by unifying parameter approach and its application to description of average critical current - bending strain relation near the average irreversible strain. Supercond. Sci. Technol. 2010; 23(2):025006.

[10] Passerini P, Dhalle' M, Giannini E, Witz G, Seeber B, Flükiger R. The influence of thermal compression on the mechanical behaviour of Ag-sheathed (Bi,Pb)2223 tapes with different matrices. Physica C 2002; 371(3),173 -84.

[11] Otto A, Harley E J, Marson R. Critical current retention in axially strained reinforced first-generation high-temperature superconducting Bi2223 wire. Supercond. Sci. Technol. 2005;18(12):S308-12.

[12] van Eck H J N, Vargast K, ten Haken B, ten Kate H H J. Bending and axial strain dependence of the critical current in superconducting BSCCO tapes. Supercond. Sci. Technol. 2002; 15(8):1213 -5.

[13] Aloysius R T, Sobha A, Guruswamy P, Samaprasad U. Bend strain and tensile stress characteristics of (Bi, Pb)-2223/Ag-Cu alloy sheathed tapes. Supercond. Sci. Technol. 2001;14(2):85 -9.

[14] Sun S J, Liu J W, Chen X P, Li M Y, Han Z. Effect of bending strain on the critical current of Bi-2223/Ag tapes with different structures. Supercond. Sci. Technol. 2003;16(9): 984 -7.

[15] Ochiai S, Shin J K, Iwamoto S, Okuda H, Oh S S, Ha D W, Sato M. Residual and fracture strains of Bi2223 filaments and their relation to critical current under applied bending and tensile strains in Bi2223/Ag/Ag alloy composite superconductor. J. Appl. Phys. 2008; 103(12):123911.

[16] Weibull W. Statistical distribution function of wide applicability. J. Appl. Mech. 1951;28:293-7.

Figure Captions

Fig.1 Transverse cross-section of the composite tape [8]. (a) shows the as-observed optical micrograph. (b) shows the modified micrograph, in which the thickness direction is enlarged by a factor of 3 from (a) and the core boundary is shown with a broken curve. (c) shows the relation of geometry of the cross-section to damage extension (when ε_B reaches $\varepsilon_{B,irr}$, damage occurs first at $y_{core}=y_{core,max}$, and when ε_B is raised from $\varepsilon_{B,irr}$ to $\varepsilon_{B,i}$ and then to $\varepsilon_{B,i+1,}$ the damage front y_f moves from $y_{core,max}$ to $y_{f,i}$ and then to $y_{f,i+1}$.)

Fig.2 Histogram of the measured I_c-values at ε_B=(a) 0, (b) 0.290 and (c) 0.338 % and plot of $\ln\ln\{1-F(I_c)\}^{-1}$ against $\ln(I_c-I_{c,min})$ for the measured I_c-values at ε_B=(a') 0, (b') 0.290 and (c') 0.338 %, where the $I_{c,min}$ values used here (63.2, 55.2 and 53.4 A at ε_B=(a') 0, (b') 0.290 and (c') 0.338 %, respectively) were estimated as the values to give the highest linearity between $\ln\ln\{1-F(I_c)\}^{-1}$ and $\ln(I_c-I_{c,min})$. Solid curves in (a), (b) and (c) show the obtained regression curves.

Fig.3 Variation of the measured $I_{c,ave}$ with ε_B. Open circles and triangles show the experimental results of the present and former [15] works, respectively. Solid curve shows the $I_{c,ave}$-ε_B relation analyzed by the damage evolution model shown later in Subsection 3.2. Distribution of I_c-values in low ε_B region, indicated with a rectangle, is analyzed in detail in Subsection 3.3.

Fig.4 Distribution of the normalized critical current (I_c/I_{c0}) values measured at ε_B=0.338%. (a) Probability density $f(I_c/I_{c0})$. (b) Plot of $\ln\ln\{1-F(I_c/I_{c0})\}^{-1}$ against $\ln(I_c/I_{c0}-0.715)$ that best-fit to the experimental results. Solid curve in (a) shows the result of regression analysis.

Fig.5 Distribution of the ε_f-ε_r values at ε_B=0.338 %. (a) Probability density $f(\varepsilon_f-\varepsilon_r)$. (a) Plot of $\ln\ln\{1-F(\varepsilon_f-\varepsilon_r)\}^{-1}$ against $\ln(\varepsilon_f-\varepsilon_r-0.130)$ that best-fits to the experimental results. Solid curve in (a) shows the result of regression analysis

Fig.6 Variation of the cumulative probability $F(\varepsilon_{B,irr})$ with irreversible bending strain $\varepsilon_{B,irr}$, corresponding to the variation of the fraction F_d (=ratio of the number of damaged specimens to that of all specimens) with bending strain ε_B. Regions (i), (ii) and (iii) refer to the bending strain ranges where no specimen is damaged (ε_B<0.148%), non-damaged and damaged specimens decrease and increase, respectively (0.148%<ε_B<0.32%) and almost all specimens are damaged (ε_B >0.32%).

Fig.7 Plot of the critical current I_c at ε_B=0.338 % against the original critical current I_{c0} at ε_B=0 %.

Fig.8 Simulation result on the variation of (a to f) I_c- and (a' to f') I_c/I_{c0}- distributions with increasing bending strain, together with the regression curves of the experimental results (taken from Figs.2(a), (b) and (c) for I_c values at ε_B=0, 0.290 and 0.338 % and from Fig.6(a) for I_c/I_{c0} values at ε_B=0.338 %), for comparison.

Fig.9 Variations of (a) average critical current $I_{c,ave}$ and normalized critical current $(I_c/I_{c0})_{ave}$ and (b) coefficient of variation of I_c- and I_c/I_{c0}-values with bending strain ε_B.

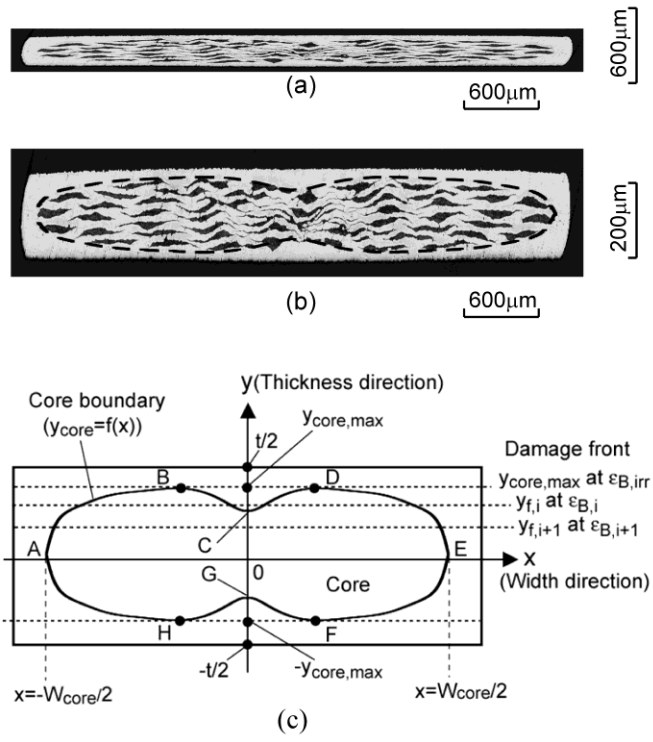
600μm
(a)
600μm
600μm
200μm
(b)
600μm
y(Thickness direction)
Core boundary
(ycore=f(x))
ycore,max
t/2
Damage front
ycore,max at εB,irr
yf,i at εB,i
yf,i+1 at εB,i+1
B
D
A
C
E
x
(Width direction)
G
0
Core
H
F
-t/2
-ycore,max
x=-Wcore/2
x=Wcore/2
(c)

Fig.1

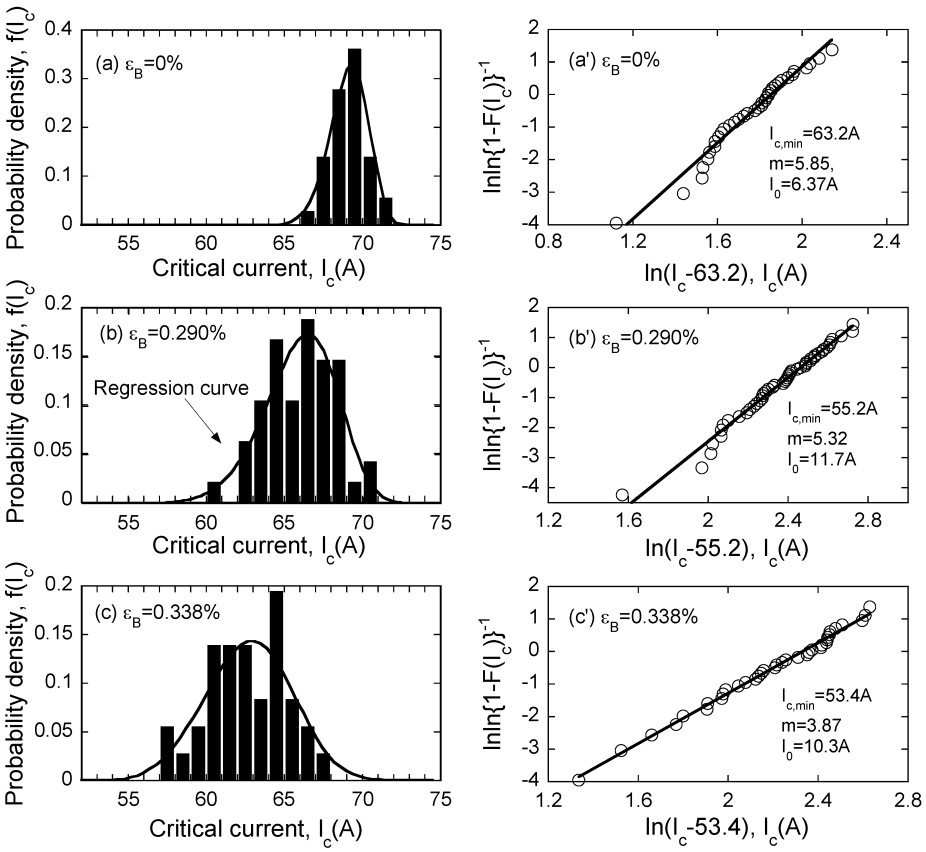
Probability density, f(Ic)
(a) εB=0%
Critical current, Ic(A)
(a') εB=0%
lnln{1-F(Ic)}-1
Ic,min=63.2A
m=5.85,
I0=6.37A
ln(Ic-63.2), Ic(A)
(b) εB=0.290%
Regression curve
(b') εB=0.290%
Ic,min=55.2A
m=5.32
I0=11.7A
ln(Ic-55.2), Ic(A)
(c) εB=0.338%
(c') εB=0.338%
Ic,min=53.4A
m=3.87
I0=10.3A
ln(Ic-53.4), Ic(A)

Fig.2

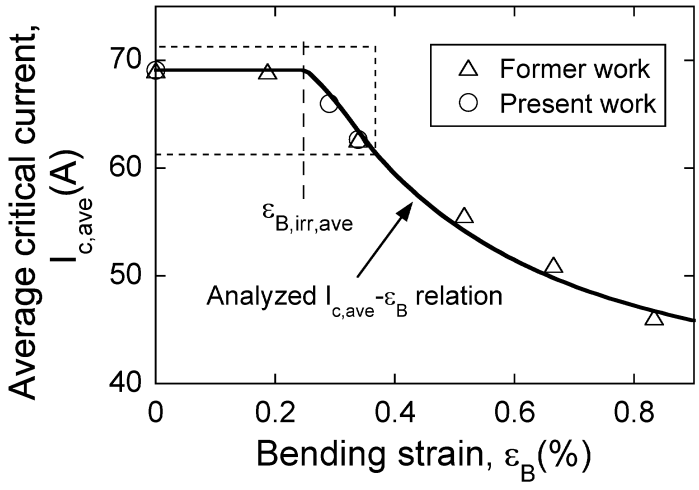
Average critical current, $I_{c,ave}$(A)
70
60
50
40
0
0.2
0.4
0.6
0.8
Bending strain, ε_B(%)
Former work
Present work
$\varepsilon_{B,irr,ave}$
Analyzed $I_{c,ave}$-ε_B relation

Fig.3

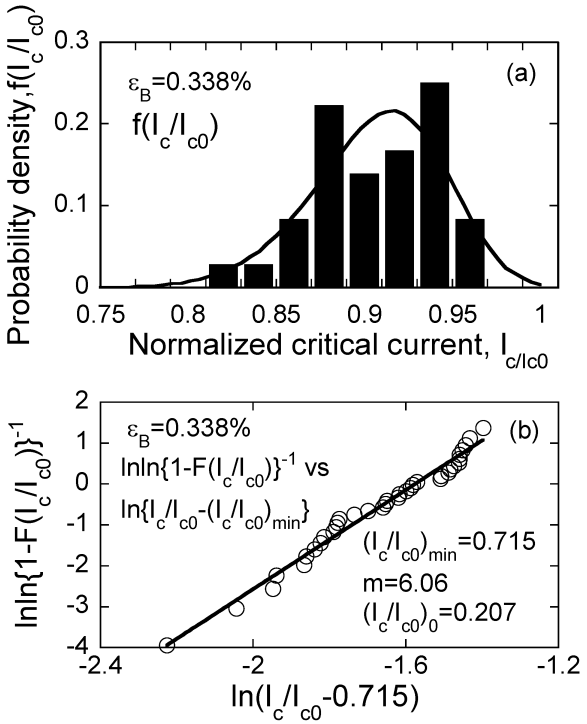
Probability density, $f(I_c/I_{c0})$
0.3
0.2
0.1
0
ε_B=0.338%
$f(I_c/I_{c0})$
(a)
0.75
0.8
0.85
0.9
0.95
1
Normalized critical current, $I_{c/Ic0}$
2
1
0
-1
-2
-3
-4
ε_B=0.338%
$\ln\ln\{1-F(I_c/I_{c0})\}^{-1}$ vs
$\ln\{I_c/I_{c0}-(I_c/I_{c0})_{min}\}$
(b)
$(I_c/I_{c0})_{min}$=0.715
m=6.06
$(I_c/I_{c0})_0$=0.207
$\ln\ln\{1-F(I_c/I_{c0})\}^{-1}$
-2.4
-2
-1.6
-1.2
$\ln(I_c/I_{c0}-0.715)$

Fig.4

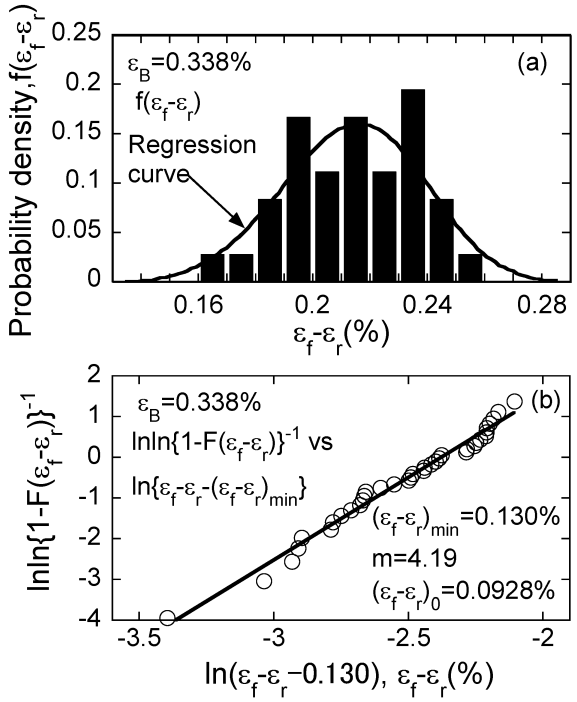
Probability density, f(εf-εr)
εB=0.338%
f(εf-εr)
Regression curve
(a)
εf-εr(%)
lnln{1-F(εf-εr)}-1
εB=0.338%
lnln{1-F(εf-εr)}-1 vs
ln{εf-εr-(εf-εr)min}
(εf-εr)min=0.130%
m=4.19
(εf-εr)0=0.0928%
(b)
ln(εf-εr−0.130), εf-εr(%)

Fig.5

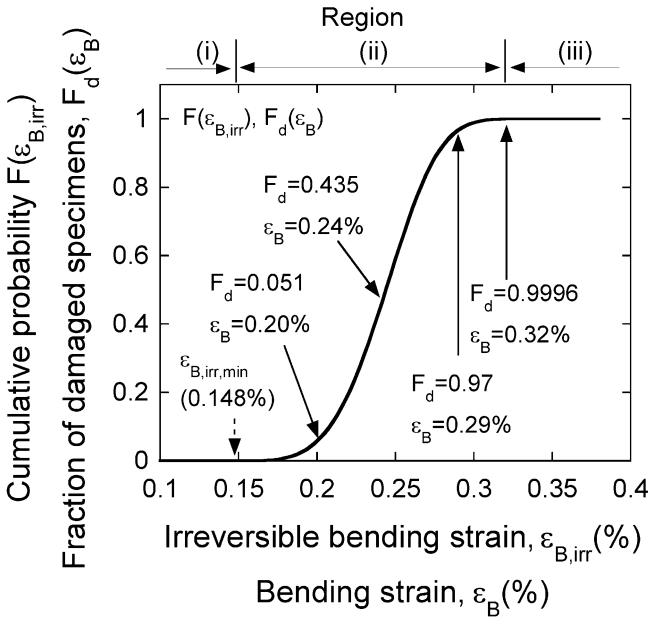
Region
(i)
(ii)
(iii)
Cumulative probability F(εB,irr)
Fraction of damaged specimens, Fd(εB)
F(εB,irr), Fd(εB)
Fd=0.435
εB=0.24%
Fd=0.051
εB=0.20%
εB,irr,min
(0.148%)
Fd=0.9996
εB=0.32%
Fd=0.97
εB=0.29%
Irreversible bending strain, εB,irr(%)
Bending strain, εB(%)

Fig.6

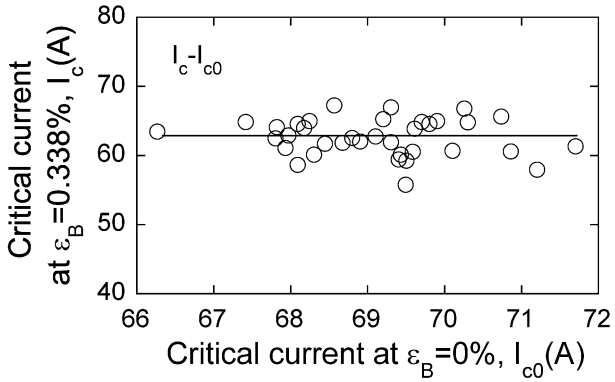
Critical current at ε_B=0.338%, I_c(A)
I_c-I_{c0}
Critical current at ε_B=0%, I_{c0}(A)

Fig.7

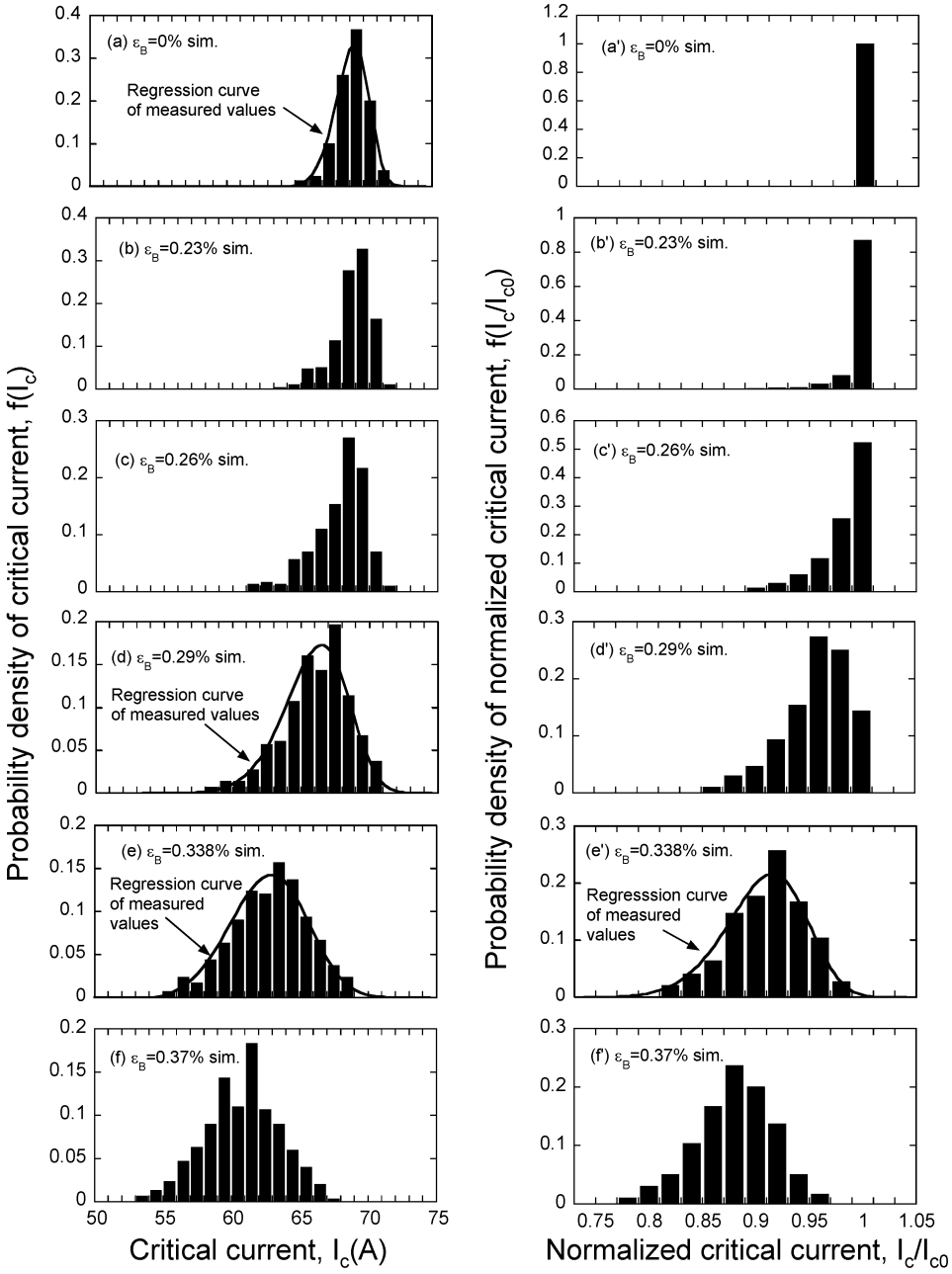
Probability density of critical current, f(I_c)
(a) ε_B=0% sim.
Regression curve of measured values
(b) ε_B=0.23% sim.
(c) ε_B=0.26% sim.
(d) ε_B=0.29% sim.
Regression curve of measured values
(e) ε_B=0.338% sim.
Regression curve of measured values
(f) ε_B=0.37% sim.
Critical current, I_c(A)
Probability density of normalized critical current, f(I_c/I_{c0})
(a') ε_B=0% sim.
(b') ε_B=0.23% sim.
(c') ε_B=0.26% sim.
(d') ε_B=0.29% sim.
(e') ε_B=0.338% sim.
Regresssion curve of measured values
(f') ε_B=0.37% sim.
Normalized critical current, I_c/I_{c0}

Fig.8

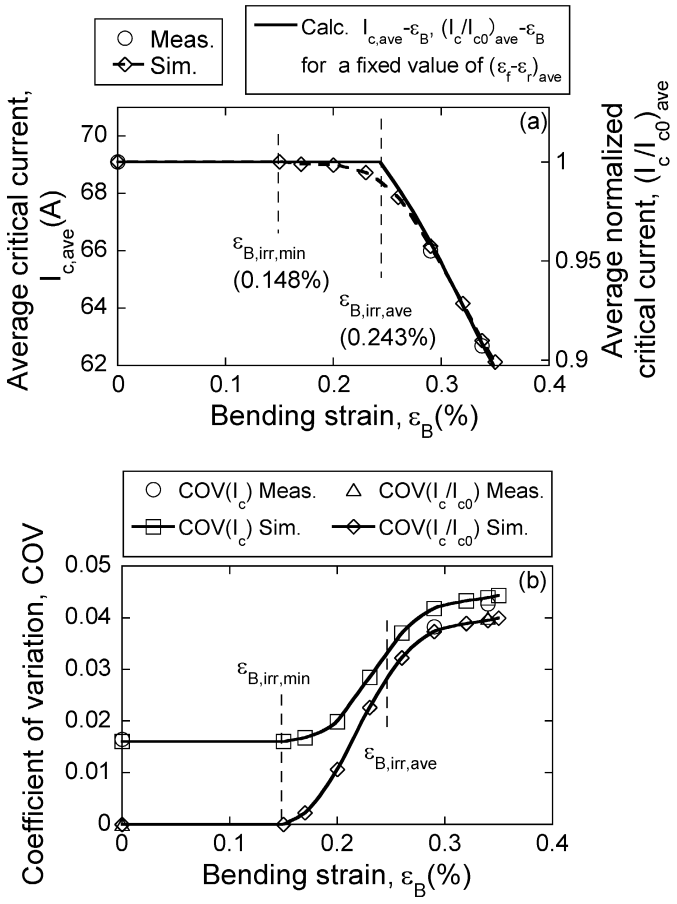
Meas.
Sim.
Calc. $I_{c,ave}$-ε_B, $(I_c/I_{c0})_{ave}$-ε_B
for a fixed value of $(\varepsilon_f-\varepsilon_r)_{ave}$
(a)
Average critical current, $I_{c,ave}$(A)
Average normalized critical current, $(I_c/I_{c0})_{ave}$
$\varepsilon_{B,irr,min}$
(0.148%)
$\varepsilon_{B,irr,ave}$
(0.243%)
Bending strain, ε_B(%)
COV(I_c) Meas.
COV(I_c/I_{c0}) Meas.
COV(I_c) Sim.
COV(I_c/I_{c0}) Sim.
(b)
Coefficient of variation, COV
$\varepsilon_{B,irr,min}$
$\varepsilon_{B,irr,ave}$
Bending strain, ε_B(%)

Fig.9